ACS OMEGA

Open Access

http://pubs.acs.org/journal/acsodf

Article

Characterization of Hydrothermally Decomposed and Synthesized $CaCO_3$ Reinforcement from Dead Snail Shells

Nanda Kumar Podaralla, Prabhu Paramasivam,* and Johan Jacquemin*

Cite This: *ACS Omega* 2024, 9, 2183−2191

Read Online

ACCESS | Metrics & More | Article Recommendations | Supporting Information

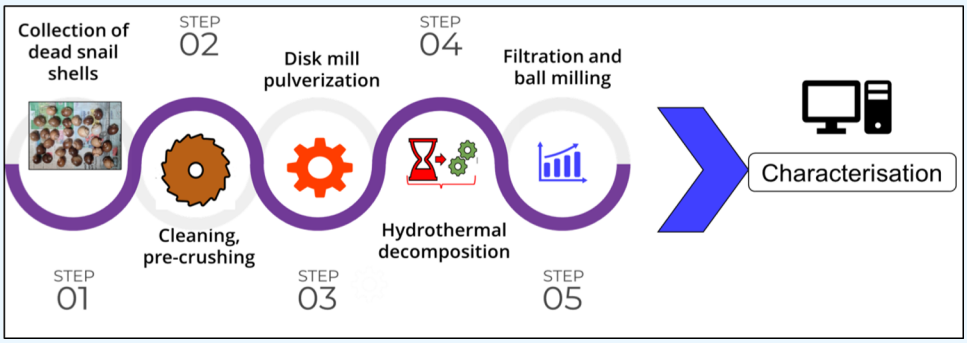

ABSTRACT: The development of new materials from marine resources presents a significant challenge due to the complexity of the associated materials and biology technologies. During this work, the snail shell, which naturally increases in thickness over time to protect the snail, has been identified as one of them. In this study, we investigated the use of powdered snail shells as a potential alternative to ceramics in the creation of customized composites. Our main objective is to explore the hydrothermal decomposition of the snail shell powder to remove undesirable components. To achieve this, we crushed and ground-washed dead snail shells and subjected them to hydrothermal decomposition using an autoclave and furnace at a temperature of 200, 220, 250, or 300 °C. We then analyzed the resulting samples using scanning electron microscope/energy-dispersive X-ray spectroscopy (SEM/EDS) and X-ray diffraction (XRD) techniques to determine changes in their composition and structure. Our findings demonstrate that all samples contained the elements Ca, C, and O, as confirmed by SEM/EDS results. XRD results show that hydrothermal decomposition at 250 °C led to good crystallization with maximum peak intensities observed at various diffraction angles. This indicates that the resulting material may have promising properties for use in composite materials. Overall, our study provides valuable insights into the use of snail shell powder as a potential material source for customized composites. Future studies could explore the optimization of the hydrothermal decomposition process and investigate the mechanical properties of the resulting materials to further develop this promising avenue of research.

1. INTRODUCTION

Biological shells, such as those from snails and seashells, are rich in hard substances, such as calcium carbonate and calcium oxides. This makes these biomaterials potential candidates as reinforcement ingredients in composite manufacturing. These biological seashells are, in fact, an attractive choice to substitute ceramic-based reinforcements. Bioshells are particularly advantageous for their strength and abundance after their life cycle, making them a valuable resource for industrial applications.[1] Biocomposites are a class of materials that are gaining popularity in industry due to their relatively low environmental impact and affordable cost. These materials are made up of natural reinforcements coupled with a resin matrix to create a sturdy and long-lasting product. Natural reinforcements, as opposed to synthetic fibers, which are commonly used in traditional composites, are generated from renewable resources and provide a more sustainable alternative. In addition, there are various advantages to using discarded snail shells in biocomposites.[2,3] For instance, the utilization of dead shells helps to reduce waste by repurposing materials that would otherwise be thrown or accumulated. Second, they are biologically created from a renewable resource. In other words, their utilization is thus an environmentally acceptable alternative to typical composite materials. Finally, this strategy is a cost-effective solution for producers looking for environmentally friendly alternatives to standard materials. To sum-up, snail shell-based biocomposites could be potentially very useful for several applications, including construction materials,

Received: July 24, 2023
Revised: November 24, 2023
Accepted: December 1, 2023
Published: January 4, 2024

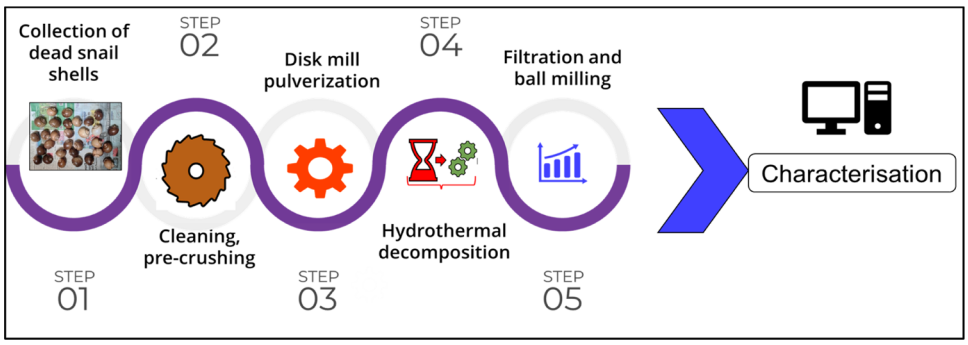

Figure 1. Flow diagram of a methodology for processing dead snail shell powder.

automobile parts, and even furniture.[4,5] These materials provide a good combination of strength, durability, and sustainability, making them an appealing alternative in a variety of industries. Biocomposites are a novel response to the growing worries about environmental pollution and sustainability.[6] Natural reinforcements, such as discarded snail shells, provide an excellent opportunity to decrease waste, develop a sustainable resource, and provide cost-effective alternatives to typical composite materials.[7,8]

Gbadeyan et al.[2] examined the microhardness and toughness of the *Achatina fulica* shell, also known as the African giant snail, under indentation stress to understand the effect of loading orientation on the prismatic and nacreous structure's hardness. This study revealed that the microhardness of the prismatic and nacreous features of the shell was dependent on the loading conditions. The load used for indenting was in the range of 50 and 500 kN, which generated tensile strengths ranging from 390 to 810 MPa and 675 to 1050 MPa nacreous and prismatic layers, respectively. Praveen et al.[9] conducted a comprehensive analysis of the chemical as well as physical properties of three species of freshwater snail shells, namely, *Pila globosa*, *Bellamya bengalensis*, and *Brotia costula*. In addition to using electron microscopy and calcium carbonate content determination techniques, the shells were also subjected to Fourier transform infrared spectroscopy (FTIR), X-ray diffraction (XRD), and energy-dispersive X-ray spectroscopy (EDS). The data obtained from the experiments showed that the $CaCO_3$ concentration in the shells varied between 87 and 96% of the total weight, depending on the species. Rihova et al.[10] conducted a study to explore the rates of shell disappearance and deterioration in nine common species of temperate European land snails. These species were selected to represent a variety of shell sizes and ecological needs. The study lasted 3 years and took place in six different forest types with varying soil pH and humidity levels. During this time, the exposed shells were monitored, and their condition was assessed at 6, 12, 24, and 36 months to calculate the rates of disappearance and deterioration, especially in the larger species. To describe the disappearance rates concerning the species and forest types, generalized linear models were used. The findings revealed that the disappearance rates of shells increased as the forests became wetter and more acidic, with smaller species bearing the greatest impact on habitat. However, independent of habitat influence, it was discovered that species size played a substantial role in the rate of disappearance and deterioration.

The utilization of dead snail shells as a potential source for the synthesis of $CaCO_3$ offers numerous benefits in terms of sustainability, waste reduction, and resource utilization. Snail shells, which are commonly discarded as waste, are a rich source of calcite and other useful compounds that can be extracted and used to produce high-quality bioceramics.[4,6] By employing the hydrothermal decomposition method, it is possible to break down the snail shells and synthesize $CaCO_3$, which can be used in a variety of applications, including in building, paper, plastics, and medicine. One of the primary advantages of using snail shells to produce $CaCO_3$ is the significant reduction in waste generated from snail shell disposal. In many regions of the world, snail shells are a major contributor to landfills, where they need almost hundreds of years to decay.[9,11,12]

In addition to reducing waste, the synthesis of $CaCO_3$ from snail shells also offers numerous benefits in terms of resource utilization.[7] Traditional $CaCO_3$ manufacturing processes rely heavily on the mining of limestone, which can have severe environmental consequences such as habitat destruction and pollution. By utilizing snail shells, which are readily available and abundant, one can reduce the need for mining and promote a more sustainable approach to resource utilization. The hydrothermal decomposition method used to synthesize $CaCO_3$ from snail shells is a highly effective and efficient process that yields high-quality bioceramics. The resulting $CaCO_3$ can be used as a reinforcement material in a variety of applications, such as plastics and building materials, where it can improve the mechanical properties and enhance product performance. Moreover, the use of $CaCO_3$ from snail shells as a filler in plastics can also contribute to reducing plastic waste, by promoting the use of recycled materials and creating a more circular economy.[13−15]

This review reveals that the hydrothermal decomposition of dead snail shells to produce $CaCO_3$ is a promising waste-to-useful-recovery strategy that offers numerous benefits in terms of sustainability, waste reduction, and resource utilization. These benefits are directly linked to the utilization of water as the main solvent, as water is recognized to be the safer and greener solvent. However, the sustainability assessment of this strategy should also consider the optimization and scalability of the given process along with the recyclability of all associated byproducts to prevent the water consumption, especially in an era when resource conservation and environmental impact are critical concerns. Given this, the present study is envisioned to explore and fine-tune this production process which has the possibility for the development of high-quality bioceramics that have significant commercial applications and contribute to a sustainable and circular economy. By following such an approach, the present study was set to explore and fine-tune the production process of an aragonite-based calcium carbonate material using dead snail shells by investigating the

https://doi.org/10.1021/acsomega.3c05330
ACS Omega 2024, 9, 2183−2191

(a) (b) (c)

Figure 2. Preprocessing samples: (a) collection of dead snail shells, (b) crushed dead snail shells before pulverization, and (c) pulverized shell powder before decomposition.

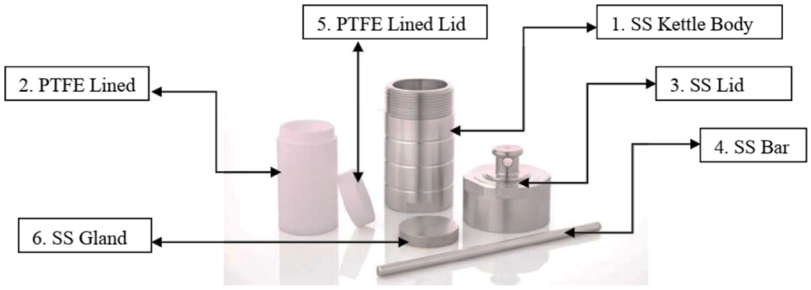

Figure 3. Basic parts of the autoclave reactor.

effects of different hydrothermal decomposition temperatures on the resulting material's composition, structure, and crystallinity.

2. MATERIALS AND METHODS

The dead snail shells are rich in $CaCO_3$. To remove impurities and convert the amorphous material into a crystallized substance, the hydrothermal decomposition process was considered. Figure 1 depicts the schematics of the process involved to eliminate impurities and improve the quality of the substance and characterization of the powder substances.

The dead snail shells were collected from the local pond bank, Mattiri Mitta, near Tada, at geolocations 13.560942 and 80.008706. Shells with an average width of 42 mm and a height of 45 mm were chosen for testing. The bucket was filled with fresh water, and the dead snail shells were added and gently stirred with a hand or a soft wooden piece to clean and remove foreign particles attached to the inner and outer sides of the shells. The water was then removed, and the process was repeated several times using fresh water until the quality was satisfactory. The cleaned shells, as shown in Figure 2a, were crushed by placing the shells in the rubber bag with the help of a wooden mallet and tapping on the top of the rubber bag. The crushed shells were again (the complexity of the geometry is simplified) cleaned with water to improve the purity of the collected material. The cleaned crushed shells, shown in Figure 2b, were further pulverized to powder using a disk milling process. The pulverized powder, shown in Figure 2c, was used for further processing their hydrothermal decomposition using an autoclave and a muffle furnace. The process of hydrothermal decomposition used during this work is explained separately below. The liquid phase contains thus water and solid matter to be separated. A cellulose filter paper with a pore size of 1 μm was placed over the top of the small container to collect water after filtration. Traditionally, the grade is used in qualitative analytical separations for precipitates. The filtered substance was then dried under air at a specific isotherm inside an autoclave until a dried powder was obtained. The abovementioned purification steps were done by drying the wet materials as a function of the temperature, i.e., at 200, 220, 250, or 300 °C. The dried and filtered powder was again placed in a planetary ball mill to get a fine powder and to remove particle agglomeration. This process was done using a ball of 3.94 mm in diameter, with a weight ratio of 1:10 and a speed of 250 rpm. The process was run 5 min clockwise and 5 min counterclockwise. After this ball milling process, the collected powders were then packed to avoid oxidation prior to be further characterized. XRD analysis was then performed to determine the crystallization and the molecular organization of each collected powder as well as the crystalline phase quantification of the $CaCO_3$ polymorphs (calcite, aragonite, vaterite) by means of the Rietveld method. The patterns were scanned through steps of 0.02 (2θ) in the 2θ range 10−90°. The full pattern refinements were carried out using the FullProf program integrated in Winplotr software. The Rietveld refinement of the observed powder XRD data was initiated with scale and background parameters, and successively, other profile parameters are included. The background was fitted with a fifth-order polynomial, while the peak shape was fitted with a pseudo-Voigt profile function. The position parameters and isotropic atomic displacement parameters of individual atoms were also refined.

Furthermore, EDS with scanning electron microscope (SEM) analysis was then performed to study the images of the crystals and to estimate the chemical elements present in each sample.

The hydrothermal autoclave reactor used during this work is based on a high-quality stainless steel closed container of 250 mL that can decompose insoluble matter. This device has an external diameter and height of 83 and 155 mm, respectively, while its internal diameter and height is close to 65 and 140 mm, respectively. This reactor, depicted in Figure 3, was used to carry out hydrothermal reactions under high pressure and temperature. A variety of poly(tetrafluoroethylene) (PTFE)

https://doi.org/10.1021/acsomega.3c05330
ACS Omega 2024, 9, 2183−2191

(a) (b) (c)

Figure 4. Steps followed during the hydrothermal decomposition. (a) Before hydrothermal decomposition. (b) After hydrothermal decomposition. (c) Filtration step realized after the hydrothermal decomposition.

Teflon-lined hydrothermal autoclave reactors were used to investigate the set hydrothermal decomposition. The weight of the powder (15 g) and the weight of the water (85 g) were taken before decomposition with a weight ratio of 15/85. After decomposition, the powder weight is 14.760 g.

3. EXPERIMENTATION

The hydrothermal decomposition process is initiated by disassembly and thorough cleaning of the parts of the autoclave. The Teflon reaction chamber is taken out and prepared to fill with reaction solvents. This will allow the top SS bottom disk or lid to be lifted and the Teflon reaction chamber to be removed. Next, the solvent (herein, water) was carefully filled into the reaction chamber, ensuring that the Teflon cap was airtight to avoid pressure leakage. It is essential to use a Teflon or PTFE liner in the stainless-steel chamber to prevent corrosion and ensure the purity of the final products. Once the liner was in place, the secondary SS locking screw cap was used for extra tightening to prevent pressure leakage.

The hydrothermal autoclave was then placed in a muffle furnace, as shown in Figure 4a and heated to reach the set temperature inside the reactor. During this work, the heating rate was set to 5 °C·min^{-1}, while the effect of the reaction temperature on the hydrothermal purification process was investigated by setting the oven temperature at 200, 220, 250, or 300 °C, as shown in Table 1. Once the hydrothermal synthesis reaction was achieved, the autoclave was then slowly cooled down inside the furnace until reaching a temperature of 40−50 °C prior to being displaced outside. The samples were then cooled down again in the open atmosphere until reaching the ambient temperature. The liquid solution was then filtered using laboratory filter paper, as shown in Figure 4c, and the liquid and solid phases were separated before further use.

Table 1. Experimental Conditions for Hydrothermal Decomposition

samples	temperature (°C)	heating time (min)
sample-1	room temperature	
sample-2	200	60
sample-3	220	60
sample-4	250	60
sample-5	300	60

The hydrothermal decomposition process is a critical step in the synthesis of materials, and it is important to follow the abovementioned steps carefully to ensure its success. Proper cleaning and maintenance of equipment, including the PTFE or Teflon liner, are also essential for reusability and cost-effectiveness. Finally, the products were then filtered prior to being dried to ensure its purity and suitability for further use.

The morphological properties and the chemical composition of the dead snail shell powder before and after the hydrothermal decomposition (samples 1 to 5) were then analyzed using the JEOL JSM-IT500 scanning electron microscope (SEM) equipped with an emission-dispersive X-ray spectroscopy technique. The Rigaku MiniFlex benchtop X-ray diffractometer is a multipurpose powder diffraction analytical instrument and was then used to determine the crystalline phase, identification (phase ID), and molecular structure. Powder XRD patterns were obtained using PAN analytical at 40 kV, 15 mA, Cu Kα radiation (= 1.5405 Å), and a scan speed of 5 min per ° in the 10−90° scan range.

4. RESULTS AND DISCUSSION

4.1. Microstructure/Elemental Composition (SEM/EDS) Results. The results of the sample morphology evolution and the elemental composition of the snail shell powders were obtained by SEM and EDS analyses. Since each tested powder is a nonconducting material, it is necessary to work in a low vacuum mode to avoid the charging effects. However, the EDS spectra, displayed in Figure 5, show that all snail shell powders (before and after hydrothermal decomposition at different set temperatures) contain the elements calcium Ca, carbon C, and oxygen O in varying amounts from theoretical values. This is probably due to the topography of the samples which may lead to the absorption of the generated X-ray of light elements like O and C, depending on the position of the analysis zone toward the EDS detector. This leads to a less accuracy of the quantification and a difference in quantification in different nonflat zones of the samples. Furthermore, it is observed that all of the samples displayed similar microstructures, mimicking a fibrous morphology. However, SEM images show that the samples are composed of fibers having a length of approximately tens of microns and equiaxed particles with grain sizes lower than 5 μm, with a mean value close to 2 μm.

By observing the SEM/EDS results, one can see that by setting the decomposition temperature at 200 °C, the collected sample has elemental values which differ slightly from theoretical values. However, by looking at the effect of the decomposition temperature, one can also see that a decomposition temperature of 250 °C led to more pronounced differences compared with other tested sample temperatures. In fact, the carbon content gradually increases with the decomposition temperature up to 250 °C, prior to decreasing by increasing the temperature to 300 °C. One can clearly see

https://doi.org/10.1021/acsomega.3c05330
ACS Omega 2024, 9, 2183−2191

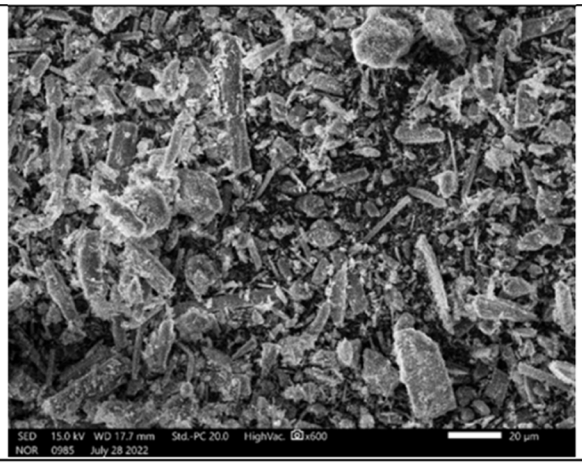

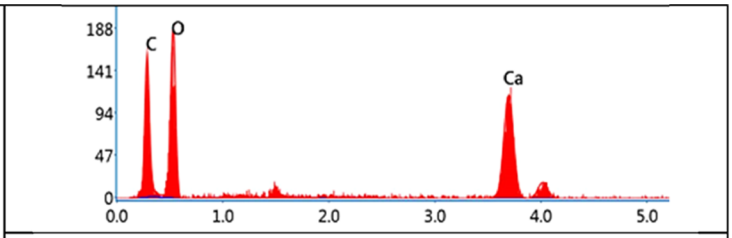

Element	Weight %	Atomic %	Error %
C K	16.5	26.2	10.16
O K	47.54	56.68	12.66
CaK	35.96	17.12	4.82

(a)

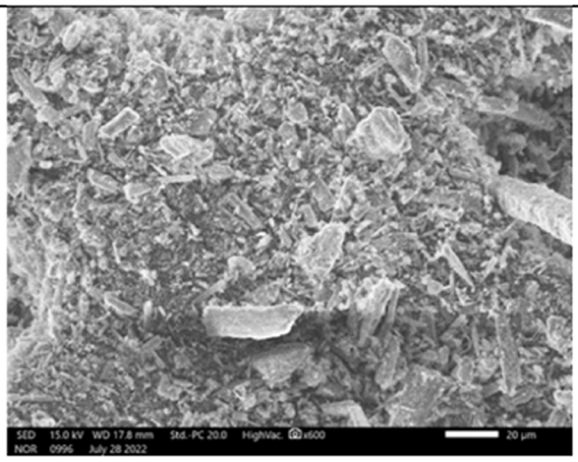

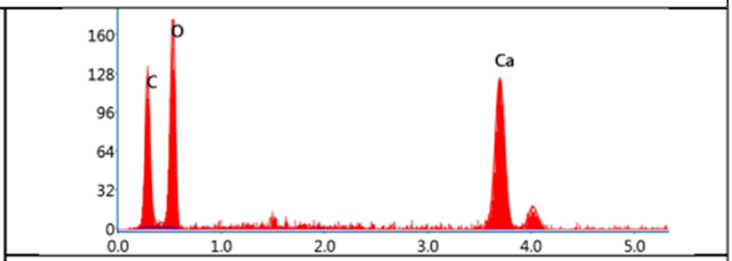

Element	Weight %	Atomic %	Error %
C K	13.58	22.43	10.8
O K	46.66	57.88	12.87
CaK	39.76	19.69	4.64

(b)

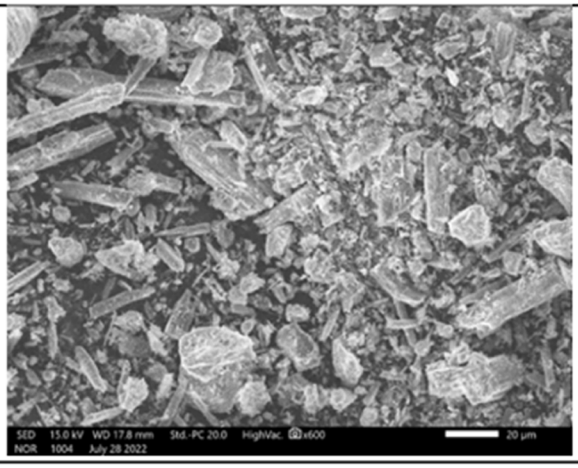

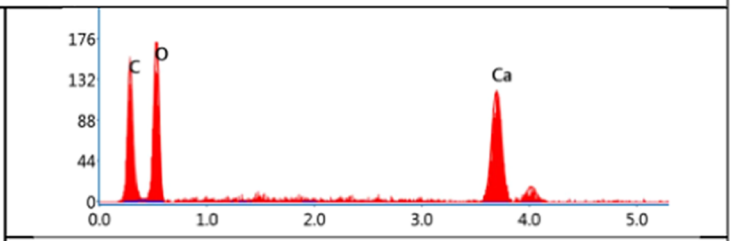

Element	Weight %	Atomic %	Error %
C K	15.36	24.92	10.42
O K	46.33	56.45	12.89
CaK	38.31	18.63	4.7

(c)

Figure 5. continued

https://doi.org/10.1021/acsomega.3c05330
ACS Omega 2024, 9, 2183−2191

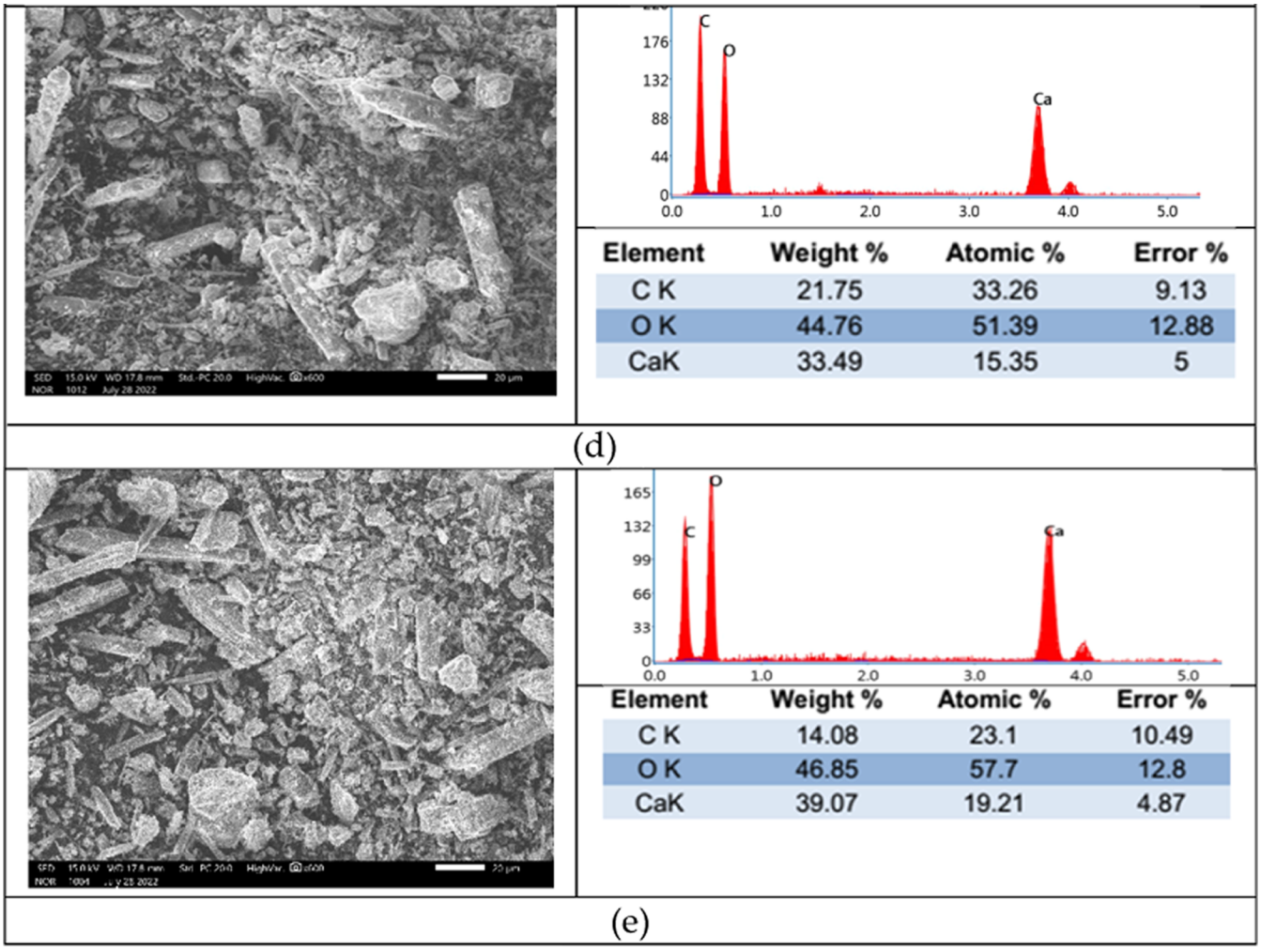

Figure 5. SEM image and EDS Spectrum of tested samples with a hydrothermal decomposition set at (a) room temperature, (b) 200 °C, (c) 220 °C, (d) 250 °C, and (e), 300 °C.

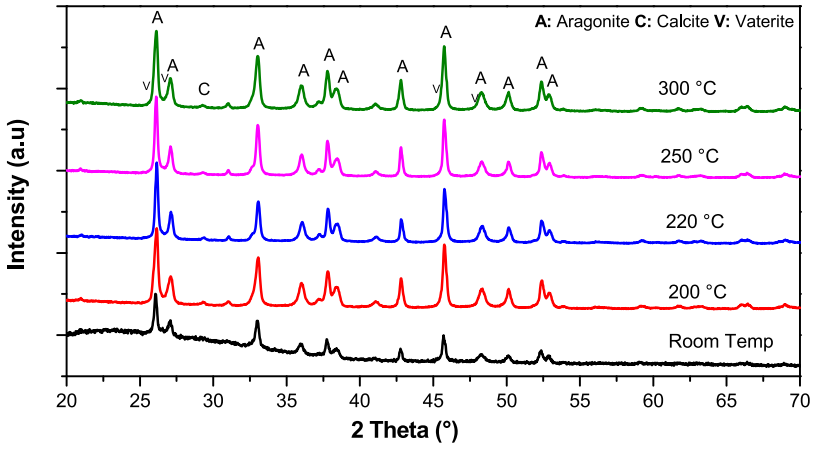

Figure 6. X-ray powder diffraction patterns of the prepared powders (RT, 200 °C, 220 °C, 250 °C, and 300 °C).

also that the C and O contents are lower when setting the hydrothermal process at 300 °C. It may be understood that temperature seems to play an important role in the material's crystallization.

4.2. X-ray Diffraction Results. *4.2.1. Qualitative Analysis of Collected XRD Patterns.* A qualitative analysis of the crystallinity of all tested samples was performed by using the Powder Diffraction File database. In fact, dead snail shell powders before and after the hydrothermal decomposition set at 200, 220, 250, or 300 °C were then tested. To study the diffraction pattern and intensities with respect to the diffraction angle, X'PERT HIGHSCORE PLUS software was used. A small amount of mismatch in the peak position and intensity is acceptable in experimental error. The XRD patterns collected

https://doi.org/10.1021/acsomega.3c05330
ACS Omega 2024, 9, 2183−2191

for all tested samples are displayed in Figures 6 and 7. The X'PERT HIGHSCORE PLUS software's search and match

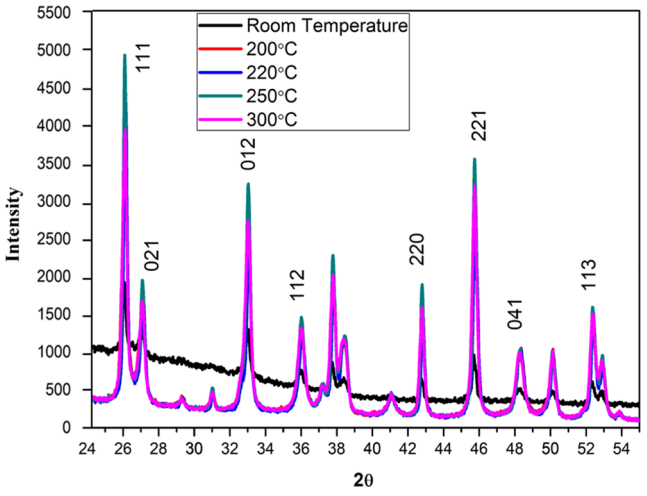

Figure 7. Overlapped patterns of XRD results collected for all tested samples between 24 and 55°.

function indicated the presence of $CaCO_3$ in the above samples, as shown in Table 2. The matching pattern and its card were taken from the reference library, and the resultant JCPDS data with reference code 00−001−0628 for calcium carbonate as aragonite with an orthorhombic structure were then selected as presented in Table 3.

Before the hydrothermal decomposition, one can see in Figure 6 that the dead snail shell powder XRD pattern is typical of an amorphous material. Furthermore, in all tested samples, no peak was observed between 10 and 25° diffraction angles, which is typical of materials displaying partial crystallinity. As the major peak is not observed in the data, that is not a good match. Minor reference peaks could be lost in the background noise; therefore, it may be acceptable if they are not observed. With reference to Table 2, the peaks at the

Table 3. JCPDS Data for Calcium Carbonate Used during This Work

ref code	score	compound name	scale factor	chemical formula
00−001−0628	62	calcium carbonate	0.669	$CaCO_3$
00−001−0628	60	calcium carbonate	0.578	$CaCO_3$
00−001−0628	56	calcium carbonate	0.495	$CaCO_3$
00−001−0628	56	calcium carbonate	0.596	$CaCO_3$

diffraction angle of the samples match the peaks at the diffraction angle of the library ref code material with a slight positive shift. The XRD peaks of dead snail shell powder were carried out, as stacked, at room temperature and at a decomposing temperature of 200, 220, 250, or 300 °C, as displayed in Figure 6. The peaks in all of the decomposed samples were observed at the same angle of diffraction. The highest peak is observed at a 26.09 to 26.14° angle of diffraction in all of the samples, with variations in the intensities presented in Figure 7. The highest peak intensity percentage of the ref code pattern also has the same diffraction angles with a minor positive shift, and the highest peak intensity percentages are also observed at the same diffraction angles.

The major peaks observed between 24 and 55° are matched in all hydrothermally decomposed samples. The maximum intensities mean the highest number of atoms that possess the highest number of electrons in the unit cell. Some peaks are the highest intensity, which means more periodicity than in other directions. The intensities increase with decomposing temperatures up to 250 °C, whereas at 300 °C, the intensity has decreased. It is observed at diffraction angles. The height of the peaks was observed in the temperature-decomposed sample at 250 °C. Hence, in that sample, a preferred crystal orientation might have developed. However, if crystals are arranged in a chaotic or random order, then the height of the peak will be low.

In the X-ray diffraction spectra of dead snail shell powder, the presence of major peaks at a diffraction angle (2) of 26.06,

Table 2. Mineralogic Phase Identification on the Investigated Samples

mineral name	chemical formula	database code	crystallographic information	RT	200 °C	220 °C	250 °C	300 °C
aragonite	$CaCO_3$	COD: 9000226	orthorhombic **S.G**: *Pmcn* a(Å) = 4.9614 b(Å) = 7.9671 c(Å) = 5.7404 $\alpha = \beta = \gamma = 90$ (deg)	major phase	major phase	major phase	major phase	major phase
vaterite	$CaCO_3$	AMCSD: 0019139	orthorhombic **S.G**: *Pbnm* a(Å) = 4.13 b(Å) = 7.15 c(Å) = 8.48 $\alpha = \beta = \gamma = 90$ (deg)	not indexed	remarkable increase	indexed	indexed	remarkable increase
calcite	$CaCO_3$	COD: 9000967	hexagonal **S.G**: $R\bar{3}c$ a(Å)= 4.984 b(Å)= 4.984 c(Å)= 17.121 $\alpha = \beta = 90$ (deg) $\gamma = 90$ (deg)	not indexed	remarkable increase	remarkable increase	remarkable increase	indexed

https://doi.org/10.1021/acsomega.3c05330
ACS Omega 2024, 9, 2183−2191

33.153, 37.80, 42.80, 45.7, and 52.38° correspond to the (111), (012), (112), (220), (221), and (113) diffraction planes as shown in Figure 7, confirming thus the formation of pure calcium carbonate crystals as suspected from SEM/EDS data.

4.2.2. Crystal Phase Quantitative and Crystal Size Evaluation Using the Rietveld Method. For the above experimental conditions, the three calcium carbonate polymorphs, i.e., the aragonite, vaterite, and calcite, could be then used when refining XRD data. The phase identification and structural investigation were then performed using collected X-ray diffraction with Cu Kα radiation as illustrated in Figure 6 with data reported in Table 2. From the XRD data, one can notice that all samples are represented as a pure calcium carbonate with the coexistence of the three polymorphs: the aragonite is represented with an orthodromic structure (space group: *Pmcn*), the vaterite structure known as a metastable phase of $CaCO_3$ that crystallizes with the orthodromic system (space group: *Pbnm*), and the calcite phase represented by an hexagonal structure (space group: $R\bar{3}c$). However, one can clearly see in Figure 6 and Table 2 that a qualitative investigation revealed the presence of argon as the major phase.

Then, for quantitative purposes, all polymorphs and their crystallographic model were taken from the crystallographic databases (see Table 2). This analysis led then to final plots, comparing the observed and calculated profiles for investigated samples, as shown in Figure 8. From this figure, one can clearly see that this quantitative analysis revealed the presence of aragonite as the major phase, i.e., representing more than 98% of each tested sample, while the remaining 2% are represented by the calcite and/or the vaterite phases, depending on the set preparation conditions.

The Scherrer's equation (eq 1) was then used for each highlighted peak of the aragonite structure in Table 4 for determining thus the crystallinity evolution of each powder as a function of the temperature. Within this analysis, the density, volume of the unit cell, and the average of the crystallite size were then determined for each tested temperature.

$$D = K\lambda/\beta \cos\theta \quad (1)$$

where D is the crystal size in nm; K is the shape factor (0.9, close to unity); β is fwhm in radians; and θ is the theta position.

According to this analysis, the effect of the set temperature on each property mimics the evolution of the peaks' intensity with the hydrothermal decomposition temperature. Each peak intensity seems to generally increase up to 250 °C, prior to the decrease as observed at 300 °C (see Table S1 and Figure S1 of the Supporting Information (SI)). From the results reported in Table S1 of the SI, the average crystal size, calculated using Scherrer's equation (eq 1), reaches the maximum value at 250 °C, as expected. This analysis reveals thus that T = 250 °C seems to be the optimum temperature to be set during the hydrothermal decomposition of dead snail shells to produce a highly crystalline aragonite-based calcium carbonate material.

5. CONCLUSIONS

The thermal decomposition of bioshell nanocomposite was realized to collect high pure samples, which were then characterized by running SEM/EDS and XRD analyses. Based on collected data, the following recommendations have been stated. The SEM/EDS results clearly highlight that before and after the hydrothermal decomposition, the snail shell powder contains mainly calcium, oxygen, and carbon, as expected. Their elemental content and contribution were strongly affected by the set hydrothermal decomposition temperature. A highest carbon content was observed by setting this process at 250 °C. Similarly, XRD results show that the observed peaks are mainly similar in terms of diffraction angles, while their intensities are also strongly affected by the set hydrothermal decomposition temperature. A quantitative analysis of the collected XRD results was thus successfully compared with JCPDS data with the card code 00−001−0628, and it was found that pure calcium carbonate with the aragonite and its orthorhombic structure reflects the main phase for each set condition. Furthermore, based on this analysis, it appears that the snail shell powder hydrothermally decomposed at 250 °C displays the highest intensity in each peak, revealing a better crystallization. In other words, one can clearly conclude that the hydrothermal decomposition was effective, thus allowing the crystallization of an amorphous material like the dead snail shell powder. Furthermore, in the light of results obtained, it appears that the best results were obtained by setting this hydrothermal decomposition at 250 °C. In fact, by analyzing collected results, one can clearly highlight that the resulting material could be considered as a bioceramic, which could be further used, in fact, to prepare biocomposites. In other words, this study provides valuable and original insights into the use of snail shell powder as a potential marine resource-based material for developing sustainable and tailored composites. However, future studies must be explored, including optimization of the hydrothermal decomposition process as well as the mechanical properties of as-prepared materials, to further evaluate this promising research approach.

■ ASSOCIATED CONTENT

Data Availability Statement

The data used to support the findings of this study are included in the articles. Should further Data or information be required, these are available on reasonable request from the corresponding author.

Supporting Information

The Supporting Information is available free of charge at https://pubs.acs.org/doi/10.1021/acsomega.3c05330.

All collected data used during the calculation of crystallite size taken from the diffraction peak of the aragonite structure by using the Rietveld calculation method (Table S1); and final plots of the observed and calculated profiles for the investigated samples as a function of the temperature (Figure S1) (PDF)

■ AUTHOR INFORMATION

Corresponding Authors

Prabhu Paramasivam − *Department of Mechanical Engineering, College of Engineering and Technology, Mattu University, Mettu 318, Ethiopia;* orcid.org/0000-0002-2397-0873; Email: prabhu.paramasivam@meu.edu.et

Johan Jacquemin − *MSN Department, Mohammed VI Polytechnic University, Benguerir 43150, Morocco;* orcid.org/0000-0002-4178-8629; Email: johan.jacquemin@um6p.ma

https://doi.org/10.1021/acsomega.3c05330
ACS Omega 2024, 9, 2183−2191

Author

Nanda Kumar Podaralla − *Mechanical Engineering Department, N.B.K.R Institute of Science & Technology, Vidyanagar 524413, India*

Complete contact information is available at: https://pubs.acs.org/10.1021/acsomega.3c05330

Author Contributions

P.N.K. conceived the research idea, provided the materials, carried experiments and prepared the samples. P.P. and P.N.K. carried out further discussion on the prepared samples and results to obtain the required data. P.N.K. carried out further laboratory experiments on the prepared samples to obtain the required data. P.P., J.J., and P.N.K. did the data analyses. P.N.K. wrote the first draft of the manuscript. J.J. and P.P. contributed to the scientific discussion of the manuscript.

Notes

The authors declare no competing financial interest.

■ ACKNOWLEDGMENTS

The authors thank the AICTE Faculty development cell (FDC). This work was supported by a grant from the AICTE of Research Project Scheme, project number F. No. 8-80/FDC/RPS (Policy-1)/2019-20. All authors would like also to thank Pr. Youssef Tamraoui and Dr. Youssef Samih, both from the MSN department of the UM6P (Morocco), for their help in the analysis of collected XRD and SEM/EDS data.

■ REFERENCES

(1) Owoyemi, H. T.; Owoyemi, A. G. Chemical and Phase Characterization of Snail Shell (Archachatina Marginata) as Bio-Waste from South-West in Nigeria for Industrial Applications. *Chem. Mater. Res.* **2020**, *12*, 15−20, DOI: 10.7176/cmr/12-6-03.

(2) Gbadeyan, O. J.; Bright, G.; Sithole, B.; Adali, S. Physical and Morphological Properties of Snail (*Achatina Fulica*) Shells for Beneficiation into Biocomposite Materials. *J. Bio- Tribo- Corros.* **2020**, *6*, No. 35, DOI: 10.1007/s40735-020-0333-6.

(3) Fattahi, A. H.; Dekamin, M. G.; Clark, J. H. Optimization of green and environmentally-benign synthesis of isoamyl acetate in the presence of ball-milled seashells by response surface methodology. *Sci. Rep.* **2023**, *13*, No. 2803, DOI: 10.1038/s41598-023-29568-y.

(4) Mo, K. H.; Alengaram, U. J.; Jumaat, M. Z.; Lee, S. C.; Goh, W. I.; Yuen, C. W. Recycling of seashell waste in concrete: A review. *Constr. Build. Mater.* **2018**, *162*, 751−764.

(5) Owuamanam, S.; Cree, D. Progress of Bio-Calcium Carbonate Waste Eggshell and Seashell Fillers in Polymer Composites: A Review. *J. Compos. Sci.* **2020**, *4*, No. 70, DOI: 10.3390/jcs4020070.

(6) Gurunathan, T.; Mohanty, S.; Nayak, S. K. A review of the recent developments in biocomposites based on natural fibres and their application perspectives. *Composites, Part A* **2015**, *77*, 1−25, DOI: 10.1016/j.compositesa.2015.06.007.

(7) Hart, A. Mini-review of waste shell-derived materials' applications. *Waste Manage. Res.* **2020**, *38*, 514−527.

(8) Upadhayay, P.; Pal, P.; Zhang, D.; Pal, A. Sea Shell Extracted Chitosan Composites and Their Applications. In *Composites from the Aquatic Environment*; Springer, 2023; pp 293−314.

(9) Parveen, S.; Chakraborty, A.; Chanda, D. K.; Pramanik, S.; Barik, A.; Aditya, G. Microstructure Analysis and Chemical and Mechanical Characterization of the Shells of Three Freshwater Snails. *ACS Omega* **2020**, *5*, 25757−25771, DOI: 10.1021/acsomega.0c03064.

(10) Říhová, D.; Janovský, Z.; Horsák, M.; Juřičková, L. Shell decomposition rates in relation to shell size and habitat conditions in contrasting types of Central European forests. *J. Molluscan Stud.* **2018**, *84*, 54−61.

(11) Zuliantoni, Z.; Suprapto, W.; Setyarini, P. H.; Gapsari, F. Extraction and characterization of snail shell waste hydroxyapatite. *Results Eng.* **2022**, *14*, No. 100390.

(12) Utami, R.; Gustiono, D.; Herdianto, N.; Roseno, S.; Effendi, M. D.; Fahyuan, H. D. In *Synthesis and Characterization of Hydroxyapatite Bioceramic from Waste of Serai Snail Shells and Mangrove Crabs for the Coast of West TanjungJabung: Effects of Sintering Temperature*, 3RD International Conference on Chemistry, Chemical Process and Engineering (IC3PE); AIP Publishing, 2021.

(13) Lu, J.; Cong, X.; Li, Y.; Hao, Y.; Wang, C. Scalable recycling of oyster shells into high purity calcite powders by the mechanochemical and hydrothermal treatments. *J. Cleaner Prod.* **2018**, *172*, 1978−1985.

(14) Komalakrishna, H.; Jyoth, T. G. S.; Kundu, B.; Mandal, S. Low Temperature Development of Nano-Hydroxyapatite from Austro-megabalanus psittacus, Star fish and Sea urchin. *Mater. Today Proc.* **2017**, *4*, 11933−11938, DOI: 10.1016/j.matpr.2017.09.114.

(15) Fatimah, I.; Aulia, G. R.; Puspitasari, W.; Nurillahi, R.; Sopia, L.; Herianto, R. Microwave-synthesized hydroxyapatite from paddy field snail (Pila ampullacea) shell for adsorption of bichromate ion. *Sustainable Environ. Res.* **2018**, *28*, 462−471.